

TWISTING CUBIC RABBITS

JUSTIN LANIER AND REBECCA R. WINARSKI

ABSTRACT. We solve an infinite family of twisted polynomial problems that are cubic generalizations of Hubbard’s twisted rabbit problem. We show how the result of twisting by a power of a certain Dehn twist depends on the 9-adic expansion of the power. For the cubic rabbit with three post-critical points, we also give an algorithmic solution to the twisting problem for the full pure mapping class group.

1. INTRODUCTION

In this paper we give closed-form and algorithmic solutions to cubic generalizations of the twisted rabbit problem. The twisted rabbit problem was formulated by Hubbard and asks: to which polynomial is $D_x^m \circ r$ Thurston equivalent? Here r is the post-critically finite quadratic polynomial known as the Douady rabbit with post-critical set P_r consisting of three points, D_x is the left-handed Dehn twist on the simple closed curve encircling the “ears” of the rabbit, and m varies over the integers. Bartholdi–Nekrashevych gave a closed-form solution to this problem, and they also gave an algorithm for determining the Thurston equivalence class of $g \circ r$ for arbitrary pure mapping classes $g \in \text{PMod}(\mathbb{R}^2, P_r)$ [1]. Their method of analyzing self-similar groups associated to post-critically finite polynomials can be used to solve other twisted polynomial problems; in the same paper they carry this out for other quadratic polynomials where the post-critical set consists of three points.

In work with Belk and Margalit, we gave an alternative solution to the twisted rabbit problem and some additional twisted polynomial problems. To do so, we followed the strategy of Bartholdi–Nekrashevych but applied methods of combinatorial topology instead of their more group theoretic approach; see [2] for a comparison of the methods. The present paper is a close sequel to Section 5 of that paper. There we gave a solution to the original twisted rabbit problem as well as an infinite family of related problems: for each n , there is an analogue of the rabbit polynomial that is a quadratic polynomial with post-critical set of size n . For each of these polynomials we defined an analogous Dehn twist cyclic subgroup and gave a closed-form solution to the associated family of twisting problems using a uniform argument.

Increasing the length of the critical cycle is one way to generalize the rabbit polynomial. Another is to change the degree of the polynomial. In this paper we consider twists of a unicritical cubic polynomial with post-critical set of size 3 called the cubic rabbit, as well as an infinite family of unicritical cubic polynomials—“many-eared” cubic rabbits—that have critical cycles of arbitrary length. In each case we give a closed-form solutions to twisting problems on a cyclic subgroup of Dehn twists. The resulting maps depend on the 9-adic expansion of the power of the twist. For the cubic rabbit with 3 post-critical points, we also give two algorithmic solutions to the problem of determining the Thurston equivalence class of post-composing the cubic rabbit with arbitrary pure mapping classes. One algorithm uses the wreath recursion approach employed by Bartholdi–Nekrashevych, while the other applies an elementary word length argument.

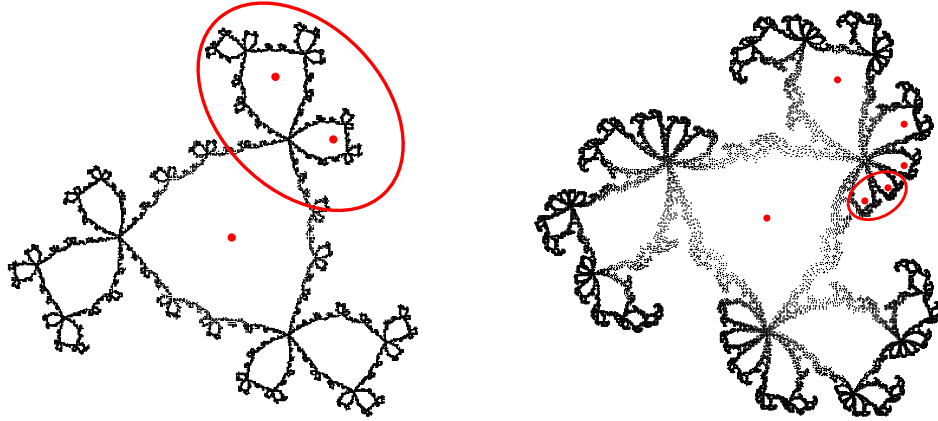


FIGURE 1. For $n = 3$ and 6 : the Julia set for R_n , the post-critical set for R_n , and the curve x_n .

In Figure 1 we depict the Julia sets and post-critical sets of cubic rabbits R_3 and R_6 with 3 and 6 post-critical points, respectively. These two polynomials are $R_n(z) = z^3 + c_n$ with $c_3 \approx 0.558 + 0.540i$ and $c_6 \approx 0.510 + 0.089i$. They belong to an infinite family R_n of polynomials that share combinatorial and dynamical properties. For each map, Figure 1 also shows a curve x_n that encircles the two points $R_n(0)$ and $R_n^2(0)$.

Up to Thurston equivalence, there are four unicritical cubic polynomials with 3 post-critical points: the cubic rabbit, the cubic airplane, and their complex conjugates. We notate these as R_3, \bar{R}_3, A_3 , and \bar{A}_3 ; see Section 3 for their descriptions. All four of these arise as twists of the cubic rabbit R_3 about the curve x_3 .

Theorem 1.1. *Let $x = x_3$ and let $m \in \mathbb{Z}$. Let s be the right-most digit in the 9-adic expansion of m that is not a 0, 4, or 8, if this exists. Then*

$$D_x^m R_3 \simeq \begin{cases} R_3 & \text{if the 9-adic expansion of } m \geq 0 \text{ contains only 0's, 4's, and 8's} \\ \bar{R}_3 & \text{if the 9-adic expansion of } m < 0 \text{ contains only 0's, 4's, and 8's} \\ A_3 & \text{if } s = 1, 5, \text{ or } 6 \\ \bar{A}_3 & \text{if } s = 2, 3, \text{ or } 7 \end{cases}$$

As illustrations of this result, the integers 89 and -77 have 9-adic expansions 108_9 and $\dots 88804_9$. (Note that $\dots 888_9 = -1$.) Therefore $D_x^{89} R_3 \simeq A_3$ and $D_x^{-77} R_3 \simeq \bar{R}_3$.

As n increases, the number of unicritical cubic polynomials with n post-critical points increases exponentially. As an organizing principle, we can find families of polynomials, indexed by n , with shared combinatorics and dynamics. The maps $D_x^m R_n$ in the “many-eared” twisted cubic rabbit problem are Thurston equivalent to polynomials in nine such families for all $n \geq 4$. We describe the families that appear in Theorem 1.2 in Section 5.

Theorem 1.2. *Let $n \geq 4$, let $x = x_n$, and let $m \in \mathbb{Z}$. If $m \neq 0$, let s be the right-most non-zero digit of the 9-adic expansion of m . Then $D_x^m R_n$ is equivalent to the map:*

	$m = 0$	$s = 1$	$s = 2$	$s = 3$	$s = 4$	$s = 5$	$s = 6$	$s = 7$	$s = 8$
$D_x^m R_n \simeq$	R_n	A_n	\bar{A}_n	$K_{n,1}$	B_n	\bar{Y}_n	$K_{n,2}$	Y_n	\bar{B}_n

To prove Theorems 1.1 and 1.2, we follow the strategy of Bartholdi–Nekrashevych [1], which consists of two main steps: producing reduction formulas and calculating base cases. Producing the reduction formulas involves lifting mapping classes through R_n . To calculate the base cases, we use the approach of Belk–Lanier–Margalit–Winarski [2] to find the topological Hubbard trees and accompanying data for a small number of twisted polynomials, to which all other cases reduce.

The 9-adic expansion of m appears in the Theorems 1.1 and 1.2 for the same reason that the 4-adic expansion of m appears in the solution of the original twisted rabbit problem: for a degree- d rabbit R with n post-critical points and a similarly situated curve x , twisting R by the mapping class $D_x^{d^2k}$ always yields the same equivalence class of topological polynomial as twisting by D_x^k . Thus powers of d^2 can be divided out of m without affecting the equivalence class of $D_x^m R$, and this is the same as dropping initial 0's in the d^2 -adic expansion m . It is possible for similar reductions to happen for other residue classes $s \pmod{d^2}$, whenever $D_x^{d^2k+s} R$ happens to be equivalent to $D_x^k R$, as shown through a lifting calculation. For these values of s , initial s 's in the d^2 -adic expansion of m can also be dropped. For both $d = 2$ and 3, additional reductions occur when $n = 3$ (the digits 4 and 8 in Theorem 1.1) but do not occur for $n \geq 4$. Forthcoming work of Mukundan and the second author further explores this phenomenon by giving solutions to twisted degree- d rabbit problems for $n = 3$ and all $d \geq 2$.

Outline of the paper. In Section 2 we review the relevant definitions and background. This includes techniques we developed with Belk and Margalit; for full details, see [2]. In Section 3 we define the cubic rabbit polynomial and prove Theorem 1.1. In Section 4 we give two algorithmic solutions to the problem of determining the Thurston equivalence class of post-composing the cubic rabbit with arbitrary pure mapping classes. In Section 5 we define the “many-eared” cubic rabbits and prove Theorem 1.2.

Acknowledgments. This work began while the authors were collaborating with Jim Belk and Dan Margalit on the paper [2]. The first author was supported by the National Science Foundation under Grant No. DGE-1650044 and Grant No. DMS-2002187. The second author was supported by the National Science Foundation under Grant No. DMS-2002951. This material is based upon work supported by the National Science Foundation under Grant No. DMS-1928930 while the second author participated in a program hosted by the Mathematical Sciences Research Institute in Berkeley, California, during Spring 2022.

2. BACKGROUND AND TECHNIQUES

We refer the reader to joint work of the authors with Belk and Margalit for additional background [2], but we review here the definitions and results essential to stating and solving our twisted cubic rabbit problems.

Topological polynomials. A *topological polynomial* f is an orientation-preserving branched cover $f : \mathbb{R}^2 \rightarrow \mathbb{R}^2$ with finite degree d greater than 1 and finitely many critical points. The *post-critical set* P_f is the forward orbit of the critical points of f . We say that a topological polynomial f is *post-critically finite* if P_f is finite.

Let $f : (\mathbb{R}^2, P_f) \rightarrow (\mathbb{R}^2, P_f)$ and $g : (\mathbb{R}^2, P_g) \rightarrow (\mathbb{R}^2, P_g)$ be topological polynomials with $|P_f| = |P_g|$. We say that f and g are *equivalent* (or *Thurston equivalent*, or *combinatorially equivalent*) if there exist orientation-preserving homeomorphisms $h_1, h_2 : (\mathbb{R}^2, P_f) \rightarrow (\mathbb{R}^2, P_g)$

such that $h_1 f = g h_2$ and h_1 and h_2 are isotopic relative to P_f . When topological polynomials f and g are equivalent, we write $f \simeq g$.

Hubbard trees. Every post-critically finite polynomial has an associated tree called its *Hubbard tree*. Let f be a polynomial with finite post-critical set P_f . Following Douady–Hubbard [3, 4], we define the Hubbard tree for f to be the union of the regulated (or allowable) arcs of P_f in the filled Julia set for f . The Hubbard tree H_f of f is invariant under f , that is, $f(H_f) \subseteq H_f$. Moreover, if f is a polynomial with Hubbard tree H_f and g is a topological polynomial that is equivalent to f , then there is an isotopy class of tree associated to g , which we obtain by pulling back H_f through the equivalence. We call this tree the *topological Hubbard tree* H_g of the topological polynomial g .

Lifting trees. Let f be a post-critically finite topological polynomial with post-critical set P_f . Let $T \subset \mathbb{R}^2$ be a tree containing P_f such that all edges of the tree are contained in a path between points in P_f . In particular, all leaves of T must lie in P_f . The *lift* of T under f is defined as a composition of two operations and is notated as $\lambda_f(T)$. First, take the preimage $f^{-1}(T)$, which is also a tree in \mathbb{R}^2 . Then take the hull relative to P_f : that is, remove any edges of $f^{-1}(T)$ that are not part of paths between points in P_f . The composition of these two operations produces a tree $\lambda_f(T)$ in \mathbb{R}^2 containing P_f . The topological Hubbard tree H_f for f is isotopic (relative to P_g) to its lift through f and so is an invariant tree for f . However, it need not be the unique tree with this property.

Tree maps and angle assignments. While the topological Hubbard tree alone is not in general sufficient to determine the equivalence class of a topological polynomial f , we can endow it with additional information that then determines the equivalence class completely. The first piece of data needed is the restriction of f to the edges of the tree. This data for instance distinguishes the rabbit and corabbit polynomials in the quadratic case and in their higher-degree generalizations. The second piece of data is an invariant angle assignment; see Poirier [11] or Belk–Lanier–Margalit–Winarski [2, Section 3] for details. This data, for instance, distinguishes what we call the airplane and the coairplane cubic polynomials.

Lifting mapping classes. We follow the strategy of Bartholdi–Nekrashevych of replacing a mapping class with its lift under a branched cover in order to determine the equivalence class of a twisted topological polynomial.

Let $f : (\mathbb{R}^2, P_f) \rightarrow (\mathbb{R}^2, P_f)$ be a branched cover and $h : (\mathbb{R}^2, P_f) \rightarrow (\mathbb{R}^2, P_f)$ be a homeomorphism. We say that h lifts under f if there exists a homeomorphism $\tilde{h} : (\mathbb{R}^2, P_f) \rightarrow (\mathbb{R}^2, P_f)$ such that $h f = f \tilde{h}$. In this case we say that h is *liftable* and that h *lifts to* \tilde{h} . Because homotopy is preserved under lifting, the homotopy classes of liftable homeomorphisms form a (finite index) subgroup of the mapping class group called the *liftable mapping class group* $\text{LMod}(\mathbb{R}^2, P_f)$.

If h lifts to \tilde{h} under f , then $h f$ and $\tilde{h} f$ are equivalent. More generally, for any $h \in \text{PMod}(\mathbb{R}^2, P_f)$, there exists g such that $g^{-1} h \in \text{LMod}(\mathbb{R}^2, P_f)$. Then $g^{-1} h$ is liftable and let $\psi(g^{-1} h)$ denote the lift. In this case, $h f$ is equivalent to $\psi(g^{-1} h) g f$ (cf. [1, Proposition 4.1] and [2, Lemma 5.1]). When f is specified, we use the notation

$$h \xrightarrow{g} \psi(g^{-1} h) g$$

to indicate equivalence obtained by choosing g as a coset representative of $h \in \text{LMod}(\mathbb{R}^2, P_f)$ and lifting. Observe that when $h \in \text{LMod}(\mathbb{R}^2, P_f)$, we may choose g to be the identity and we suppress g in the notation.

For f a topological polynomial and g and h mapping classes, whenever $gf \simeq hf$ we say $g \sim h$, where it is understood that this is with respect to the map f .

A criterion for trivial lifts. To find the result of lifting a curve, one can simply take the preimage and forget the inessential components. However, there exists a useful criterion that guarantees that the preimage of a curve will have only inessential components. To this end, we prove a generalization of Lemma 5.2 in Belk–Lanier–Margalit–Winarski [2], extending it to topological polynomials of degree higher than 2. We first require some definitions.

Let f be a unicritical topological polynomial of degree d . A *branch cut* b for f is a arc in (\mathbb{R}^2, P_f) connecting the critical value of f to ∞ . The preimage $f^{-1}(b)$ is a union of d arcs that intersect only at the critical point. The complement of $f^{-1}(b)$ in \mathbb{R}^2 has d components. We say that b is a *special branch cut* for f if all points in P_f lie in the same component of $f^{-1}(b)$. A special branch cut for R_3 (and R_n , similarly) is the straight arc from the critical value to ∞ that avoids the interior of the triangle determined by P_{R_3} ; this is depicted as the arc b in Figure 3.

Let c be a simple closed curve that is isotopic to the boundary of a disk D that contains exactly two marked points. A *defining arc* for c is a simple arc contained in D that has an endpoint at each marked point in D . Up to isotopy, there is a unique defining arc for any such c .

Lemma 2.1. *Let f be a topological polynomial of degree d and let b be a special branch cut for f . Suppose c is a curve in (\mathbb{R}^2, P_f) that surrounds exactly two points of P_f , neither of which is the critical value, and that a is a defining arc for c . If the algebraic intersection number of a and b is not 0 mod d , then the lift of D_c is trivial.*

See the discussion of the reduction formulas in Section 3 for an illustrated application of this lemma. Recall that a curve is trivial if it is homotopic to a point (or a boundary component). The Dehn twist about a curve γ is trivial if and only if γ is trivial.

Proof. Since c does not surround the critical value of f , the arc a does not have an endpoint at the critical value. Therefore $f^{-1}(a)$ consists of d arcs that are disjoint, including at their endpoints. Since the algebraic intersection number of a and b is not 0 mod d , the endpoints of each component of $f^{-1}(a)$ lie in different connected components of $\mathbb{R}^2 \setminus f^{-1}(b)$. Since a nontrivial arc must have the property that both of its endpoints are in the same connected component of $\mathbb{R}^2 \setminus f^{-1}(b)$ (the component containing P_f), all arcs of $f^{-1}(a)$ are trivial. The lift $\psi(D_c)$ is equal to the product of the Dehn twists about the curves of the boundary of a neighborhood of $f^{-1}(a)$. Since each such curve surrounds at most one point of P_f , this product is trivial. \square

3. TWISTING THE CUBIC RABBIT

Every unicritical cubic polynomial is affine conjugate to a polynomial of the form $f(z) = z^3 + c$ with critical point 0. There are eight distinct non-zero solutions to the equation $(c^3 + c)^3 + c = 0$, each of which yields a post-critically finite cubic polynomial with critical portrait $0 \rightarrow c \rightarrow c^3 + c \rightarrow 0$. These eight polynomials come in four equivalent pairs; each pair is affine conjugate under the map $z \rightarrow -z$. We take as representatives of these four equivalence classes the following four polynomials, which we call the cubic rabbit R_3 , the

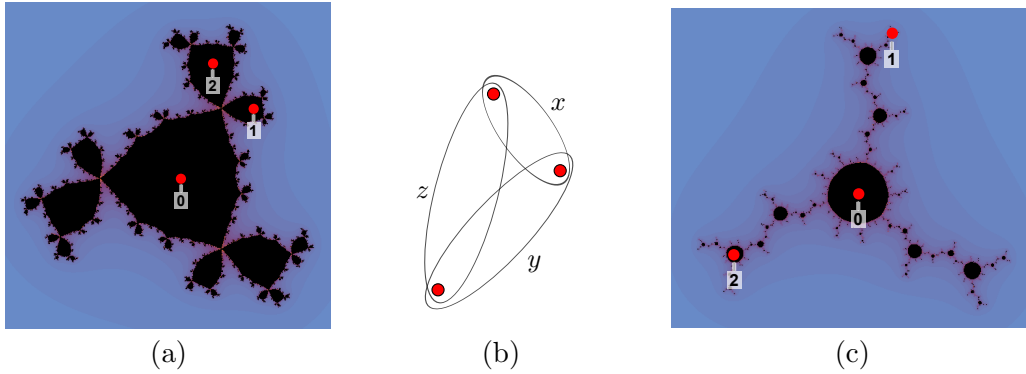


FIGURE 2. (a) The Julia set for the cubic rabbit R_3 . (b) The curves x , y , and z in (\mathbb{R}^2, P_{R_3}) . (c) The Julia set for the cubic airplane A_3 .

cubic corabbit \overline{R}_3 , the cubic airplane A_3 , and the cubic coairplane \overline{A}_3 . These polynomial representatives have the form $z^3 + c$, where the four approximate values of c are $0.558 + 0.540i$, $0.558 - 0.540i$, $.264 + 1.260i$, and $.264 - 1.260i$, respectively. The Julia sets for R_3 and A_3 are depicted in Figure 2.

Also depicted in Figure 2 three curves x , y and z lying in (\mathbb{R}^2, P_{R_3}) ; they are analogues of the curves in the original twisted rabbit problem. The curve x is obtained as the boundary of a regular neighborhood of the straight line segment between $\text{Rot}_3(0)$ and $\text{Rot}_3^2(0)$.

By the Berstein–Levy theorem, a topological polynomial with all post-critical points in a critical cycle is unobstructed [8]. Therefore the composition of a pure mapping class with R_3 must be equivalent to one of R_3 , \overline{R}_3 , A_3 , or \overline{A}_3 . In particular, this is true for all maps $D_x^m R_3$.

We now describe a topological polynomial that is homotopic (and so also equivalent) to R_3 using techniques of combinatorial topology. We describe the map topologically in order to lift isotopy classes of trees and curves through R_3 without the need to compute images of analytic maps. Let $P_{R_3} = \{0, R_3(0), R_3^2(0)\}$ be the post-critical set of R_3 , and let Δ be the solid triangle in \mathbb{R}^2 with vertex set P_{R_3} . Let Cub be any orientation-preserving triple branched cover $(\mathbb{R}^2, P_{R_3}) \rightarrow (\mathbb{R}^2, P_{R_3})$ that is branched over 0 and that fixes Δ pointwise. Any such map fixes any tree contained in Δ . By the Alexander method, there are two isotopy classes relative to the set P_{R_3} of such branched covers, and these branched covers are equivalent (relative to the set P_{R_3}). Let Rot_3 be a homeomorphism of (\mathbb{R}^2, P_{R_3}) that rotates the points

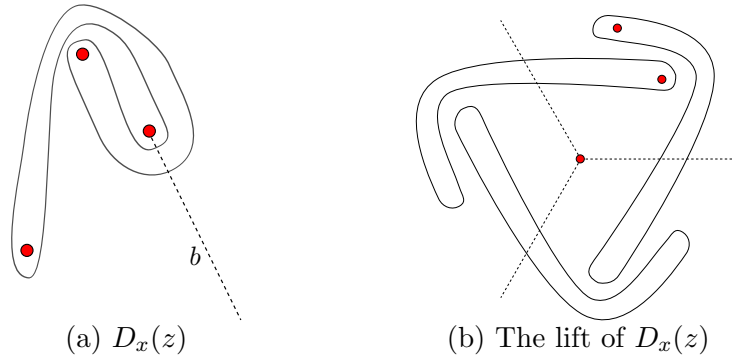


FIGURE 3. In general, the defining arc for $D_x^k(z)$ intersects b in k points.

P_{R_3} counterclockwise and preserves Δ as a set. Any two such maps are isotopic relative to P_{R_3} . Then the map $\text{Rot}_3 \circ \text{Cub}$ is homotopic to the cubic rabbit polynomial relative to P_{R_3} ; this is straightforward to check using the Alexander method (cf. [2, Proposition 3.1]).

3.1. Reduction formulas. We are now ready to explain the first of the two steps in our solution to the twisted cubic rabbit problem. The reduction formulas are:

$$D_x^m R_3 \simeq \begin{cases} D_x^k R_3 & m = 9k \\ D_x R_3 & m = 9k + 1 \\ D_x^2 R_3 & m = 9k + 2 \\ D_y R_3 & m = 9k + 3 \\ D_x^k R_3 & m = 9k + 4 \\ D_x R_3 & m = 9k + 5 \\ D_y^2 R_3 & m = 9k + 6 \\ D_x^{-2} R_3 & m = 9k + 7 \\ D_x^k R_3 & m = 9k + 8 \end{cases}.$$

To verify these formulas, we apply a number of facts about lifting individual curves and their corresponding Dehn twists through R_3 . For instance, the curve z has three preimages under R_3 , and the only essential one is homotopic to x . Therefore, as in the original twisted rabbit problem, D_z is in $\text{LMod}(\mathbb{R}^2, P_{R_3})$ and we have $D_z \rightsquigarrow D_x$. The preimage of x has a single component, isotopic to y . Therefore D_x is not in $\text{LMod}(\mathbb{R}^2, P_{R_3})$, but D_x^3 is in $\text{LMod}(\mathbb{R}^2, P_{R_3})$ and $D_x^3 \rightsquigarrow D_y$. Similarly $D_y^3 \rightsquigarrow D_z$. We illustrate this lifting process for several additional curves in Figures 3 and 4.

We now give an example of Lemma 2.1 in action, showing that $D_x^k D_z D_x^{-k} = D_{D_x^k(z)} \rightsquigarrow \text{id}$ for $k \not\equiv 0 \pmod{3}$ (similarly, $D_{D_y^k(z)} \rightsquigarrow \text{id}$ for $k \not\equiv 0 \pmod{3}$). Figure 3 illustrates the case $k = 1$. Indeed, let a be the defining arc of z . Then a is disjoint from the special branch cut b and intersects x only once. Therefore the geometric intersection of b with $D_x^k(a)$ is $\pm k$ (this is a special case of [5, Proposition 3.4] for arcs). In this situation, the absolute value of the algebraic intersection of $D_x^k(a)$ and b is the same as the geometric intersection because all intersections between b and $D_x^k(a)$ arise from twisting a about x in the same direction. The same argument applies to $D_y^k(z)$.

We are now prepared to justify the reduction formulas.

Case 1: $m = 9k$. In this case we have

$$D_x^{9k} = (D_x^3)^{3k} \rightsquigarrow D_y^{3k} = (D_y^3)^k \rightsquigarrow D_z^k \rightsquigarrow D_x^k.$$

Thus $D_x^{9k} \sim D_x^k$, as desired.

Case 2: $m = 9k + 1$. In this case we require one additional fact, namely that $D_{D_x^{-1}(y)}^3 \rightsquigarrow D_z$. This follows from the fact that the preimage of the curve $D_x^{-1}(y)$ has a single component, which is isotopic to z ; see Figure 4. We have

$$D_x^{9k+1} \xrightarrow{D_x} D_y^{3k} D_x \xrightarrow{D_x} D_z^k D_x \xrightarrow{D_x} \psi(D_{D_x^{-1}(z)}^k) D_x = D_x.$$

Thus, $D_x^{9k+1} \sim D_x$, as desired.

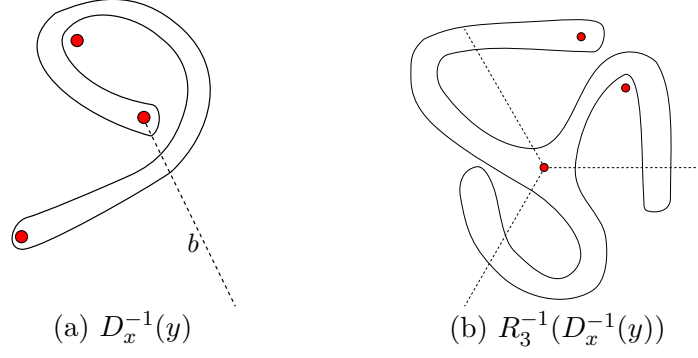


FIGURE 4. The curve $R_3^{-1}(D_x^{-1}(y))$ is homotopic to z .

Case 3: $m = 9k + 2$. In this case we use the fact that the preimage of the curve $D_x^{-2}(y)$ has a single component, which is isotopic to z .

$$D_x^{9k+2} \underset{\sim}{\overset{D_x^2}{\rightsquigarrow}} D_y^{3k} D_x^2 \underset{\sim}{\overset{D_x^2}{\rightsquigarrow}} D_z^k D_x^2 \underset{\sim}{\overset{D_x^2}{\rightsquigarrow}} \psi(D_{D_x^{-2}(z)}^k) D_x^2 = D_x^2.$$

Thus $D_x^{9k+2} \sim D_x^2$ as desired.

Case 4: $m = 9k + 3$. We have

$$D_x^{9k+3} \rightsquigarrow D_y^{3k+1} \underset{\sim}{\overset{D_y}{\rightsquigarrow}} D_z^k D_y \underset{\sim}{\overset{D_y}{\rightsquigarrow}} \psi(D_{D_y^{-1}(z)}^k) D_y = D_y.$$

Thus, $D_x^{9k+3} \sim D_y$, as desired.

Case 5: $m = 9k + 4$. In this case we have

$$D_x^{9k+4} \underset{\sim}{\overset{D_x}{\rightsquigarrow}} D_y^{3k+1} D_x = D_y^{3k} D_x^{-1} D_z^{-1} D_x = D_y^{3k} D_{D_x^{-1}(z)}^{-1} \rightsquigarrow D_z^k \rightsquigarrow D_x^k,$$

where we used the lantern relation in the first equality. Then both D_y^{3k} and $D_{D_x^{-1}(z)}^{-1}$ lift, where the latter lifts to the identity by Lemma 2.1. Thus, $D_x^{9k+4} \sim D_x^k$, as desired.

Case 6: $m = 9k + 5$. We use two facts that have not previously appeared. First, the preimage of $D_x(y)$ is a single component that is homotopic to $D_y(z)$. Second, the curve defining arc of $D_x D_y^2(z)$ has algebraic intersection 1 with b , therefore the preimage of $D_x D_y^2(z)$ is trivial by Lemma 2.1. We have

$$\begin{aligned} D_x^{9k+5} \underset{\sim}{\overset{D_x^{-1}}{\rightsquigarrow}} D_y^{3k+2} D_x^{-1} \underset{\sim}{\overset{D_y^{-1} D_x^{-1}}{\rightsquigarrow}} \psi(D_x D_y^{3k+3} D_x^{-1}) D_y^{-1} D_x^{-1} &= (D_y D_z^{k+1} D_y^{-1}) D_y^{-1} D_x^{-1} \\ \underset{\sim}{\overset{D_y^{-1} D_x^{-1}}{\rightsquigarrow}} \psi(D_x D_y^2 D_z^{k+1} D_y^{-2} D_x^{-1}) D_y^{-1} D_x^{-1} &= D_y^{-1} D_x^{-1} = D_z \rightsquigarrow D_x \end{aligned}$$

where the final equality is an application of the lantern relation. Thus, $D_x^{9k+5} \sim D_x$, as desired.

Case 7: $m = 9k + 6$. We have:

$$D_x^{9k+6} \rightsquigarrow D_y^{3k+2} \underset{\sim}{\overset{D_y^2}{\rightsquigarrow}} D_z^k D_y^2 \underset{\sim}{\overset{D_y^2}{\rightsquigarrow}} \psi(D_{D_y^{-2}(z)}^k) D_y^2 = D_y^2.$$

Thus, $D_x^{9k+6} \sim D_y^2$, as desired.

Case 8: $m = 9k + 7$. In this case we use the fact that the preimage of $D_x^2(y)$ consists of single connected component, which is homotopic to $D_x^{-1}(z)$. We have:

$$D_x^{9k+7} \xrightarrow{\sim} D_y^{3k+3} D_x^{-2} \xrightarrow{\sim} D_{D_x^{-1}(z)}^{k+1} D_x^{-2} \xrightarrow{\sim} \psi(D_x^2 D_{D_x^{-1}(z)}^{k+1} D_x^{-2}) D_x^{-2} = \psi(D_{D_x(z)}^{k+1}) D_x^{-2} = D_x^{-2}.$$

Thus, $D_x^{9k+7} \sim D_x^{-2}$, as desired.

Case 9: $m = 9k + 8$. In this case we use the fact that the preimage of the curve $D_x(y)$ consists of single connected component, which is homotopic to $D_y(z)$. We also apply the lantern relation to show that $D_x D_y(z) = z$. We have

$$D_x^{9k+8} \xrightarrow{\sim} D_y^{3k+3} D_x^{-1} \xrightarrow{\sim} D_{D_y(z)}^{k+1} D_x^{-1} \xrightarrow{\sim} \psi(D_x D_{D_y(z)}^{k+1} D_x^{-1}) D_x^{-1} = \psi(D_z^{k+1}) D_x^{-1} = D_x^k.$$

Thus, $D_x^{9k+8} \sim D_x^k$, as desired.

3.2. Base cases. The second step in our proof of Theorem 1.1 is to determine the polynomials to which the maps $D_x R_3$, $D_x^2 R_3$, $D_y R_3$, $D_y^2 R_3$, and $D_x^{-2} R_3$ are equivalent.

The Hubbard trees for R_3 and \bar{R}_3 are tripods and the Hubbard trees for A_3 and \bar{A}_3 are paths of length 2. This can be seen from their Julia sets, as shown in Figure 2. As discussed in Section 2, the Hubbard tree, an invariant angle assignment on the tree, and the dynamical map on the edges of the tree induced by the polynomial, suffice to determine the polynomial. The polynomial R_3 maps the edges of its Hubbard tree (a tripod) counterclockwise, while \bar{R}_3 maps the edges of its Hubbard tree clockwise. In both cases the angles at the leaves are 2π and the angles at the vertex of valence 3 each have measure $\frac{2\pi}{3}$. The polynomial A_3 supports an invariant angle assignment where the counterclockwise angle from edge e_1 and to edge e_2 is $2\pi/3$, while for \bar{A}_3 this angle is $4\pi/3$. In each case, e_1 is the edge from the critical point 0 and the critical value.

Therefore, in order to determine the equivalence class of gR_3 for $g \in \text{PMod}(\mathbb{R}^2, P_{R_3})$, we first find a tree that is invariant under the lifting map. If it is a path of length 2 that supports an invariant angle assignment, then this is the topological Hubbard tree for gR_3 and the map is equivalent to either A_3 or \bar{A}_3 ; the invariant angle assignment distinguishes between the two possibilities. Moreover, the invariant angle assignment can be recovered from the full preimage: the critical value is a leaf of the topological Hubbard tree, and therefore the single angle adjacent to it has measure 2π . In the full preimage of the topological Hubbard tree, the critical point is trivalent, and each adjacent angle will have measure $\frac{2\pi}{3}$. Because the critical point is bivalent in the topological Hubbard tree, one of the edges of the full preimage is not in the hull. When this edge is removed, the angle on the side of the topological Hubbard tree from which the extra edge was removed will have angle $\frac{4\pi}{3}$. If the invariant tree for gR_3 is instead a tripod, then this is the topological Hubbard tree for the map and the direction in which the dynamical map on the edges of the tree rotates the edges distinguishes between the two possibilities R_3 and \bar{R}_3 .

Proof of Theorem 1.1. If $m \geq 0$ and the 9-adic expansion of m contains only 0's, 4's, and 8's, then the reduction formulas reduce $D_x^m R_3$ to R_3 .

If $m < 0$ and the 9-adic expansion of m contains only 0's, 4's, and 8's, the reduction formulas reduce m to $\dots 888 = -1$. So in this case we have $D_x^m R_3 \simeq D_x^{-1} R_3$. The topological Hubbard tree for $D_x^{-1} R_3$ is shown in Figure 5. Since $D_x^{-1} R_3$ maps the edges of this tripod clockwise (relative to the trivalent point), we have $D_x^{-1} R_3 \simeq \bar{R}_3$.

If there exists a digit in the 9-adic expansion of m that is not 0, 4, or 8, let s be the first such digit. Then the reduction formulas determine that $D_x^m R_3$ is equivalent to one of: $D_x R_3$,

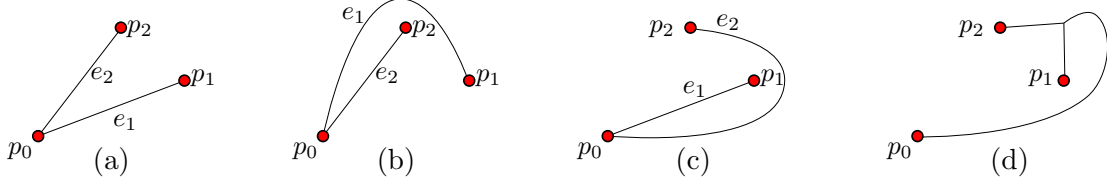


FIGURE 5. (a) The topological Hubbard tree for $D_x R_3$ and $D_x^2 R_3$. (b) The topological Hubbard tree for $D_y R_3$ and $D_y^2 R_3$. (c) The topological Hubbard tree for $D_x^{-2} R_3$. (d) The topological Hubbard tree for $D_x^{-1} R_3$.

$D_x^2 R_3$, $D_y R_3$, $D_y^2 R_3$, or $D_x^{-2} R_3$, depending on s . The topological Hubbard tree for each of these base cases is depicted in Figure 5. Each of these topological Hubbard trees is a path of length 2, so the corresponding maps are equivalent to either A_3 or \bar{A}_3 . Further, the trees for $D_x R_3$ and $D_y^2 R_3$ support an invariant angle assignment with angle $\angle(e_1, e_2) = 2\pi/3$, and so $D_x R_3$ is equivalent to A_3 . Similarly, the trees for $D_x^2 R_3$, $D_y R_3$ and $D_x^{-2} R_3$ support an angle structure with angle $\angle(e_1, e_2) = 4\pi/3$, and so $D_x^2 R_3$ is equivalent to \bar{A}_3 . (Angles are measured counterclockwise from e_1 to e_2). \square

4. THE GENERAL SOLUTION FOR THE TWISTED CUBIC RABBIT

In this section we describe two closely related algorithms for determining the equivalence class of gR_3 , where g is an arbitrary pure mapping class in $\text{PMod}(\mathbb{R}^2, P_{R_3})$. We first give a “whole word” algorithm that is directly analogous to the one given by Bartholdi–Nekrashevych for the quadratic rabbit [1, Section 4.1]. The proof we give for this algorithm follows their approach via the theory of self-similar groups. Second, we give a “prefix” algorithm and justify it through an elementary argument using word length. Finally, we give some computational results of applying these algorithms.

4.1. Whole-word algorithm. The pure mapping class group $\text{PMod}(\mathbb{R}^2, P_{R_3})$ is a free group generated by D_x and D_z as a free basis. There is an index 3 subgroup $\text{LMod}(\mathbb{R}^2, P_{R_3}) < \text{PMod}(\mathbb{R}^2, P_{R_3})$ consisting of elements that are liftable through R_3 to pure mapping classes. This subgroup is generated by the following elements:

$$\mathcal{L} = \{D_x^3, D_z, D_x^{-1}D_zD_x, D_xD_zD_x^{-1}\}$$

In the previous section we showed the following facts:

$$D_x^3 \rightsquigarrow D_y = D_x^{-1}D_z^{-1} \quad D_z \rightsquigarrow D_x \quad D_x^{-1}D_zD_x \rightsquigarrow id \quad D_xD_zD_x^{-1} \rightsquigarrow id.$$

These facts yield a homomorphism $\psi : \text{LMod}(\mathbb{R}^2, P_{R_3}) \rightarrow \text{PMod}(\mathbb{R}^2, P_{R_3})$.

We can extend the homomorphism ψ to a well-defined set map $\bar{\psi}$ from $\text{PMod}(\mathbb{R}^2, P_{R_3})$ to itself as follows:

$$\bar{\psi} : g \mapsto \begin{cases} \psi(g), & g \in \text{LMod}(\mathbb{R}^2, P_{R_3}) \\ \psi(D_x^{-1}g)D_x, & D_x^{-1}g \in \text{LMod}(\mathbb{R}^2, P_{R_3}) \\ \psi(D_xg)D_x^{-1}, & D_xg \in \text{LMod}(\mathbb{R}^2, P_{R_3}) \end{cases}$$

By [2, Lemma 5.1], we have: that $gR_3 \simeq \bar{\psi}(g)R_3$ for all $g \in \text{PMod}(\mathbb{R}^2, P_{R_3})$.

Wreath recursions. Following Bartholdi–Nekrashevych [1, Proposition 4.2], we encode the map $\bar{\psi}$ using a wreath recursion; see their Section 2.2 for additional background. Note that our convention of function composition notation runs opposite to their group theoretic notation. A wreath recursion is a homomorphism $\Phi : G \rightarrow G \wr \Sigma_n$ where G is a group and Σ_n is a symmetric group acting on $X = \{1, \dots, n\}$. We write elements of the wreath product in the form $\sigma \langle \langle g_n, \dots, g_1 \rangle \rangle$, with $\sigma \in \Sigma_n$ and $g_i \in G$. If σ is the identity in Σ_n or if all of the g_i are the identity in G , these may be suppressed in the notation. Multiplication in the wreath recursion is carried out through two rules. First, two adjacent elements in angle brackets are multiplied in the group G entrywise: $\langle \langle h_n, \dots, h_1 \rangle \rangle \langle \langle g_n, \dots, g_1 \rangle \rangle = \langle \langle h_n g_n, \dots, h_1 g_1 \rangle \rangle$. Second, an element σ acts by permutation on the indices of the g_i when pushed past an angle bracket term: $\langle \langle g_n, \dots, g_1 \rangle \rangle \sigma = \sigma \langle \langle g_{\sigma(n)}, \dots, g_{\sigma(1)} \rangle \rangle$. For a wreath recursion Φ and $g \in G$, the restriction map $g|_i$ is the i th coordinate of $\Phi(g)$. Restriction maps can be composed; inductively we put $g|_{xv} = (g|_v)|_x$ for all $x \in X$ and $v \in X^*$, the set of finite words in X .

A benefit of this coding is that wreath recursions have a simple criterion that determines when there exists a finite set to which the restriction map contracts under iteration (i.e. a nucleus): a self-similar action of a group G with finite symmetric generating set S (with $1 \in S$) is contracting if and only if there exists a finite set $\mathcal{N} \subset G$ and a number $k \in \mathbb{N}$ such that $((S \cup \mathcal{N})^2)|_{X^k} \subseteq \mathcal{N}$ [10, Lemma 2.11.2]. The GAP package AutomGrp can be used to compute the nucleus of a contracting wreath recursion [9].

Theorem 4.1. *Iterating $\bar{\psi}$ on an element $g \in \text{PMod}(\mathbb{R}^2, P_{R_3})$ yields exactly one member of the following set: $\{id, D_x, D_x^{-1}, D_z D_x^2\}$. The equivalence class of gR_3 is then determined as follows:*

$$gR_3 \simeq \begin{cases} R_3, & \text{if } \bar{\psi}^n(g) = id \\ \bar{R}_3, & \text{if } \bar{\psi}^n(g) = D_x^{-1} \\ A_3, & \text{if } \bar{\psi}^n(g) = D_x \\ \bar{A}_3, & \text{if } \bar{\psi}^n(g) = D_z D_x^2 \end{cases}$$

Proof. Consider the wreath recursion $\Phi : \text{PMod}(\mathbb{R}^2, P_{R_3}) \rightarrow \text{PMod}(\mathbb{R}^2, P_{R_3}) \wr \Sigma_3$ given by

$$\Phi(D_x) = \rho \langle \langle D_x^{-1} D_z^{-1}, id, id \rangle \rangle \quad \text{and} \quad \Phi(D_z) = \langle \langle id, id, D_x \rangle \rangle$$

where ρ is the permutation (132): $\rho(1) = 3$, $\rho(3) = 2$, $\rho(2) = 1$.

This wreath recursion encodes the map $\bar{\psi}$; computing $\bar{\psi}(g)$ is the same as computing $g|_1$, and then adjusting the result according to the value of the accompanying permutation factor. For $g \in \mathcal{L}$, we have that $\bar{\psi}(g) = g|_1$ and that $\Phi(g)$ has trivial permutation factor; since Φ is a homomorphism, the same is true for all $g \in \text{LMod}(\mathbb{R}^2, P_{R_3})$. In the case where $D_x^{-1}g \in \text{LMod}(\mathbb{R}^2, P_{R_3})$, we have that $\Phi(g) = \rho \langle \langle g_3, g_2, g_1 \rangle \rangle$ and

$$\bar{\psi}(g) = \psi(D_x^{-1}g)D_x = (D_x^{-1}g)|_1 D_x = (\rho^2 \langle \langle id, D_z D_x, id \rangle \rangle \rho \langle \langle g_3, g_2, g_1 \rangle \rangle)|_1 D_x = g|_1 D_x$$

Similarly, in the case where $D_x g \in \text{LMod}(\mathbb{R}^2, P_{R_3})$, we have $\bar{\psi}(g) = g|_1 D_x^{-1}$. Since $D_x|_1 = D_x^{-1}|_1 = id$, we have by induction for all $n \in \mathbb{N}$ that

$$\bar{\psi}^n(g) = g|_v \quad \text{or} \quad \bar{\psi}^n(g) = g|_v D_x \quad \text{or} \quad \bar{\psi}^n(g) = g|_v D_x^{-1} \quad \text{for some } v \in X^n.$$

A small computation yields the following nucleus set for the restriction map for Φ :

$$\mathcal{N} = \{id, D_x, D_x^{-1}, D_z D_x, D_x^{-1} D_z^{-1}\}$$

Therefore for all $g \in \text{PMod}(\mathbb{R}^2, P_{R_3})$ we have that $\bar{\psi}^n(g) \in \mathcal{N} \cup D_x^{-1} \cup D_x$ for all sufficiently large n . It then suffices to analyze the dynamics of $\bar{\psi}$ acting on this finite set; the only cycles are the fixed points id , D_x , and D_x^{-1} and the 2-cycle on $D_z D_x^2$ and $D_x^{-1} D_z^{-1} D_x^{-1}$. Taking

$D_z D_x^2$ as the representative for the 2-cycle yields the four elements $\{id, D_x, D_x^{-1}, D_z D_x^2\}$ in the theorem statement. The computations of the base cases in Section 3 then yield the result, since $D_x R_3 \simeq A_3$ and $D_x^{-1} R_3 \simeq \overline{R_3}$ are among these, while $D_z D_x^2 \sim D_x^{-2}$ and $D_x^{-2} R_3 \simeq \overline{A_3}$. \square

4.2. Prefix algorithm. Any $g \in \text{PMod}(\mathbb{R}^2, P_{R_3})$ of reduced word length at least 4 in the free generating set $\{D_x, D_z\}$ can be subdivided into two pieces $g = hp$ where h is possibly the empty word and p is one of the eight prefixes (or inverted variants thereof) as shown in Table 1.

Case	$g = hp$	g'	$\Delta = g' - g $
1)	hD_z	$D_x h$	$\Delta \leq 0$
2)	hD_x^3	$D_x^{-1} D_z^{-1} h$	$\Delta \leq -1$
3)	$hD_x^{-1} D_z D_x$	h	$\Delta = -3$
4)	$hD_x D_z D_x^{-1}$	h	$\Delta = -3$
5)	$hD_z D_x = hD_x D_x^{-1} D_z D_x$	hD_x	$\Delta = -1$
6)	$hD_x D_z D_x D_x = hD_x D_z D_x^{-1} D_x^3$	$D_x^{-1} D_z^{-1} h$	$\Delta \leq -2$
7)	$hD_x^{-1} D_z D_x D_x = hD_x D_x^{-2} D_z D_x^2$	hD_x	$\Delta \leq -3$
8)	$hD_z D_z D_x D_x = hD_x^{-1} D_x D_z D_z D_x^{-1} D_x^3$	$D_x^{-1} D_z^{-1} h D_x^{-1}$	$\Delta \leq -1$

TABLE 1. The eight cases of prefixes for words in $\text{PMod}(\mathbb{R}^2, P_{R_3})$ of length at least 4 and the effects of lifting these through R_3 on reduced word length.

In each case the prefix p may be lifted through R_3 (perhaps with borrowing) and then the lift may be appended to h . This yields a new word g' , and by the same logic as [2, Lemma 5.1] we have that $g' R_3 \simeq g R_3$. In the first four cases p itself is liftable; each is a generator in \mathcal{L} . In the sixth case p can be rewritten as a product of two of these generators. In the remaining three cases borrowing is required in order to lift p . The change in reduced word length in each case is recorded in Table 1; the fact that in some cases we have an inequality for this change comes from the fact that the new word may admit free reduction.

Let $P(g) = g'$ be the prefix lifting map just described, which is well defined on all $g \in \text{PMod}(\mathbb{R}^2, P_{R_3})$ of reduced word length at least 4, as well as for some shorter words. For the remaining reduced words in $g \in \text{PMod}(\mathbb{R}^2, P_{R_3})$ of length at most 3, we define $P(g) = g$. We do this for the sake of making the algorithm as simple as possible, although the trade-off is that there are more terminal words than is necessary. (The issue is that further lifting shows that some of these short words are in the same equivalence class, but this further lifting does not necessarily decrease reduced word length.) We now show that iterating the map P yields an algorithm for determining the equivalence class of $g R_3$.

Theorem 4.2. *For any $g \in \text{PMod}(\mathbb{R}^2, P_{R_3})$, there exists a $k \geq 0$ such that $|P^k(g)| < 4$. Moreover, for any g , there exists an k such that $P^k(g)$ is one of the following nine values, and the equivalence class of $g R_3$ is determined by the corresponding value in Table 2.*

Proof. If $|g| < 4$, the first statement holds trivially. Then let $g \in \text{PMod}(\mathbb{R}^2, P_{R_3})$ be a reduced word of length at least 4. We show that for some $k > 0$ we have $|P^k(g)| < |g|$; the first statement will then hold by induction. If the prefix of g falls into one of the cases 2

$P^k(g) =$	id	D_x	D_x^{-1}	D_x^2	D_x^{-2}	$D_z D_x^2$	$D_z D_x^{-2}$	$D_z^{-1} D_x^2$	$D_z^{-1} D_x^{-2}$
$gR_3 \simeq$	R_3	A_3	\bar{R}_3	\bar{A}_3	\bar{A}_3	\bar{A}_3	\bar{A}_3	\bar{A}_3	\bar{A}_3

TABLE 2. The nine terminal words under iterates of P on $\text{PMod}(\mathbb{R}^2, P_{R_3})$ and the corresponding equivalence classes of gR_3 .

through 8 in Table 1, we have that $\Delta \leq -1$ and so we have the desired decrease in reduced word length with $k = 1$. Otherwise, we are in Case 1 and $g = hD_z$ (or, similarly, $g = hD_z^{-1}$). Then $g' = D_x h$ and reduced word length may not have decreased, but it has not increased, and now there is a new prefix. Further applications of P do not increase word length and eventually produce a word that begins with D_x or D_x^{-1} . Note that every word g' in Table 1 begins with either h or D_x or D_x^{-1} , and that even in the situation where g is a power of D_z , applications of P eventually produce a power of D_x . Thus Case 1 reduces to the other cases.

It remains to consider the dynamics of P on words of length at most 3. The only cycles are the 9 fixed points recorded in Table 2 along with the corresponding equivalence classes of gR_3 . Again, these were either computed as base cases in Section 3 or (in the case of the five words yielding \bar{A}) are shown to be equivalent to a base case with a small amount of direct calculation. \square

Computations. Recall that the group $\text{PMod}(\mathbb{R}^2, P_{R_3})$ is a free group of rank 2. With the generating set $\{D_x, D_z\}$ it contains $2 \cdot 3^\ell - 1$ elements of reduced word length at most ℓ . In Table 3 we give the counts of these elements according to their equivalence classes gR_3 for small values of ℓ . We have computed these results using both the whole-word and prefix algorithms. Note that the tallies given in the chart are dependent on the chosen generating set.

ℓ	0	1	2	3	4	5	6	7	8	9
R_3	1	1	3	11	27	94	287	857	2527	7341
\bar{R}_3	0	2	4	8	29	82	258	785	2294	6802
A_3	0	2	4	12	48	139	445	1367	4078	12495
\bar{A}_3	0	0	6	22	57	170	467	1364	4222	12727

TABLE 3. The relative frequency of R_3 , \bar{R}_3 , A_3 and \bar{A}_3 for gR_3 with $|g| \leq \ell$ in the generating set $\{D_x, D_z\}$

It would be interesting to know whether there is a limiting ratio among the equivalence classes as ℓ goes to infinity, and if so, what this ratio is. To our knowledge an exact result along these lines is not known even in the case of the quadratic rabbit. Answers to these questions would represent a significant step forward in the study of twisted polynomial problems.

5. TWISTING THE MANY-EARED CUBIC RABBIT

We now turn to many-eared cubic rabbits R_n , the analogues of the cubic rabbit but where the critical portrait is a cycle of n marked points. We begin by giving a combinatorial description of the maps R_n , just as we did for R_3 . We then describe the families of topological polynomials that arise in Theorem 1.2, the solution of the twisted many-eared cubic rabbit problem. We then solve this problem in two steps, first producing reduction formulas and then determining the base cases.

The Hubbard tree for R_n is depicted in Figure 6. Labeling the edges so that e_i has p_i as one of its endpoints, the induced map of R_n on the edges of its Hubbard tree is:

$$(R_n)_*(e_i) = \begin{cases} e_{i+1} & 0 \leq i \leq n-1 \end{cases}$$

with indices taken mod n . The complex kneading sequence for the family R_n is $\overline{11 \cdots 1*}$. The polynomials in the family R_n also have n -pods as their Hubbard trees, but $\overline{R_n}$ rotates the edges of these n -pods clockwise instead of counterclockwise. The complex kneading sequence for $\overline{R_n}$ is also $\overline{11 \cdots 1*}$.

We now give a combinatorial topology description of a map that is homotopic to R_n relative to P_{R_n} , and so also equivalent to R_n . For the post-critical set P_{R_n} , let $0 = p_0$ be the origin and let the points p_i be $R_n^i(0)$ for $1 \leq i \leq n-1$. Let Δ_n denote the solid n -gon with vertex set P_{R_n} . Let Cub be any triple branched cover $(\mathbb{R}^2, P_{R_n}) \rightarrow (\mathbb{R}^2, P_{R_n})$ that is only branched over 0 and fixes pointwise Δ_n . Let Rot_n be a homeomorphism of (\mathbb{R}^2, P_{R_n}) that rotates the points P_{R_n} counterclockwise, with each p_i mapping to p_{i+1} , and that preserves Δ_n setwise. This homeomorphism is unique up to homotopy relative to P_{R_n} . Then $\text{Rot}_n \circ \text{Cub}$ is homotopic to R_n , for each value of n , as follows. The n -pod contained in Δ_n is invariant under lifting by $\text{Rot}_n \circ \text{Cub}$ and $\text{Rot}_n \circ \text{Cub}$ permutes the edges counterclockwise. Moreover, the n -pod satisfies Poirier's conditions to be the topological Hubbard tree for $\text{Rot}_n \circ \text{Cub}$. Since the Hubbard tree for R_n is a homotopic n -pod relative to P_{R_n} and R_n permutes the edges counterclockwise, R_n and $\text{Rot}_n \circ \text{Cub}$ are homotopic. This is again an application of the Alexander method.

For any fixed n , let the curve c_i be the boundary of a regular neighborhood of the straight arc from p_{i-1} to p_i with indices taken mod n . Set $x = c_2$, $y = c_1$, and $z = c_0$. These curves are also depicted in Figure 6.

5.1. The required polynomial families. We now describe the polynomials that appear in the statement of Theorem 1.2. These polynomials fall in nine families, three of which are in complex conjugate pairs. That is, one family in the pair is a sequence of polynomials $z^3 + c_n$ while the other is a sequence of polynomials $z^3 + \overline{c_n}$. While the corresponding maps in the families are not equivalent, they are conjugate via the orientation-reversing homeomorphism of complex conjugation. Therefore it suffices to give descriptions in detail of six families. For each of the families, we provide multiple pieces of identifying information: the kneading sequence, the Hubbard tree and the dynamical map on the edges, the angle at the critical point, and the direction of rotation of the post-critical set. This data is redundant, but we hope that readers with different mathematical tastes will find their preferred descriptions. Note that the Hubbard trees are depicted schematically. The complex kneading sequence, defined by Hubbard–Schleicher [6], is in the cubic case a string of digits in the set $\{0, 1, 2, *\}$ that describes the *itinerary* of the post-critical points relative to the unit circle. (See Kauko [7] for a definition of higher-degree kneading sequences and details of the convention we use). In what follows, we name the critical point p_0 and $p_i = f^i(p_0)$ for $1 \leq i \leq n-1$.

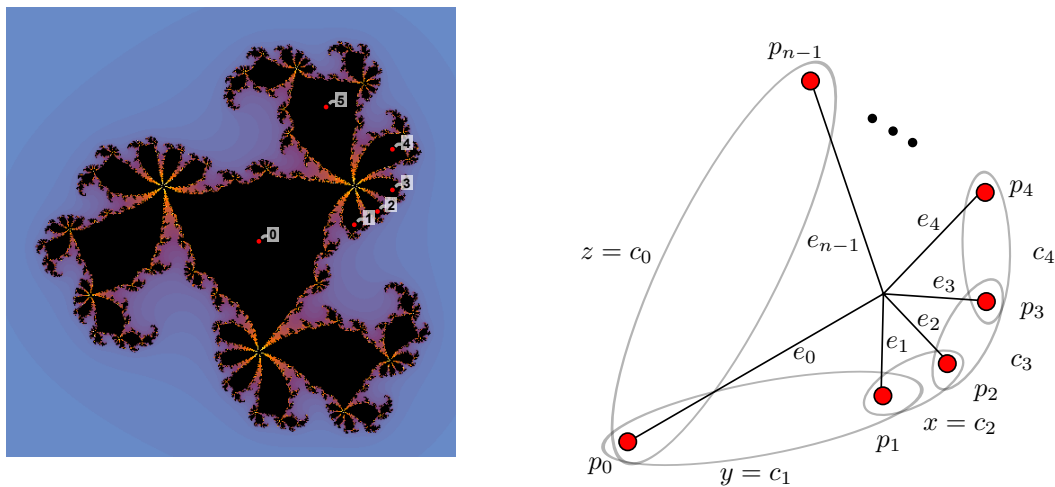


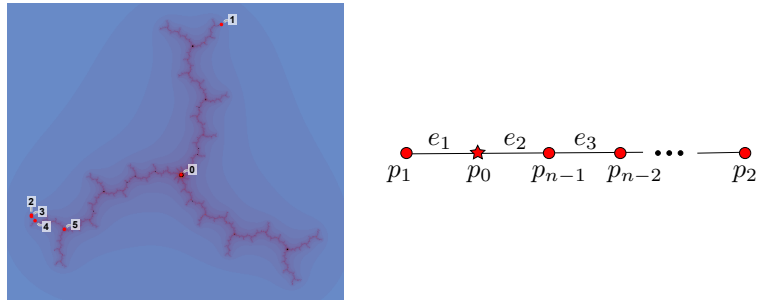
FIGURE 6. The Julia set for R_6 . The Hubbard tree and the curves c_i for R_n .

Five of the families of polynomials that arise in our solution are cubic analogues of families that appeared in the quadratic twisted many-eared rabbit problem. The first of the families is R_n and we will call the other four A_n , B_n , $K_{n,1}$ and $K_{n,2}$, as in Belk–Lanier–Margalit–Winarski [2, Section 5]. The maps $K_{n,1}$ and $K_{n,2}$ are both generalizations of the quadratic Kokopelli family K_n . As in the quadratic case, the Hubbard trees for the families A_n and B_n are paths of length $n - 1$. Unlike the quadratic case, the families A_n and B_n do not have real coefficients; note that their Hubbard trees do not lie in the real line and their post-critical sets do not lie on a line, although we depict them in this way.

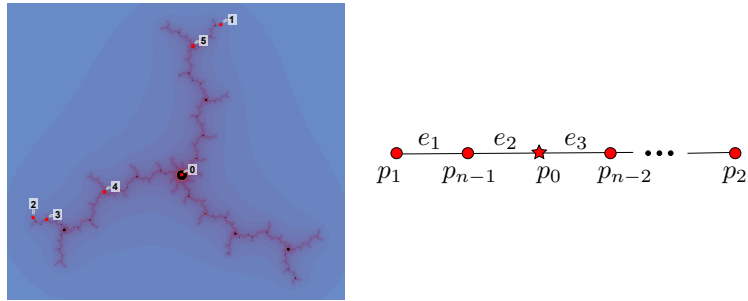
The family A_n . After R_n , the second family of polynomials is A_n . The Hubbard tree for A_n is depicted in Figure 7a and the induced map on the edges is:

$$(A_n)_*(e_i) = \begin{cases} e_1 e_2 \cdots e_{n-1} & i = 1 \\ e_{i-1} & 2 \leq i \leq n - 1 \end{cases}.$$

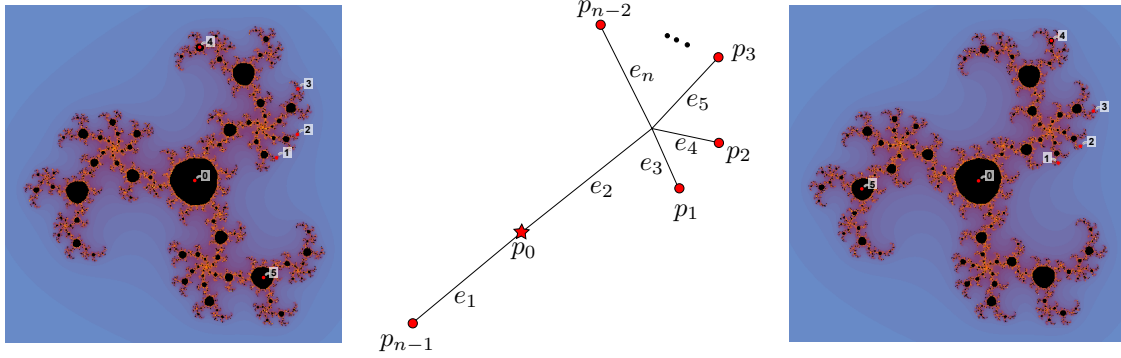
The complex kneading sequence for the family A_n is $\overline{122 \cdots 2^*}$. There is a homeomorphism between the Hubbard tree for A_n and a subset of the real line such that p_1 is to the left of p_0 and p_2, \dots, p_{n-1} are to the right of p_0 . As in the 2-eared cubic rabbit case, let e_1 be the edge between p_0 and p_1 , and let e_2 be the edge between p_0 and p_{n-1} . The angle in A_n measured counterclockwise from e_1 to e_2 is $2\pi/3$. This is indicated in the kneading sequence because the second digit is one more than the first, which encodes the fact that p_2 is one sector counterclockwise from p_1 . The polynomial $\overline{A_n}$ has the same Hubbard tree as A_n , but the invariant angle between e_1 and e_2 (measured counterclockwise) is $4\pi/3$. The complex kneading sequence for $\overline{A_n}$ is $\overline{10 \cdots 0^*}$.



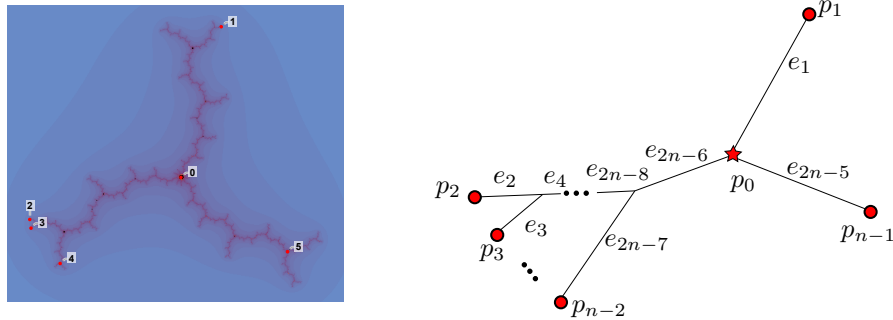
(A) The Julia set for A_6 and the Hubbard tree for A_n



(B) The Julia set for B_6 and the Hubbard tree for B_n



(C) The Julia set for $K_{6,1}$. The Hubbard tree for $K_{n,1}$ and $K_{n,2}$. The Julia set for $K_{6,2}$.



(D) The Julia set for Y_6 and the Hubbard tree for Y_n

FIGURE 7. The Julia sets for $A_6, B_6, K_{6,1}, K_{6,2}$ and Y_6 and the Hubbard trees for the corresponding families.

The family B_n . The third family is B_n . The Hubbard tree for B_n is also a path of length $n - 1$, depicted in Figure 7b. The induced map on the edges is given by:

$$(B_n)_*(e_i) = \begin{cases} e_3 \cdots e_{n-1} & i = 1 \\ e_1 e_2 & i = 2 \\ e_1 & i = 3 \\ e_2 e_3 & i = 4 \\ e_{i-1} & 5 \leq i \leq n - 1 \end{cases} .$$

The cubic complex kneading sequence of B_n is $\overline{12 \cdots 21^*}$ (the intermediate digits are all 2). There is a homeomorphism between the Hubbard tree for B_n and subset of the real line such that p_1 and p_{n-1} are to the left of p_0 and all the other post-critical points are to the right of p_0 . We name the edges e_1, \dots, e_{n-1} from left to right in this embedding. Then e_2 and e_3 are the edges that meet at the critical point. The (counterclockwise) angle between e_2 and e_3 has measure $2\pi/3$. This is indicated in the kneading sequence because the $n - 1$ st digit is one less than the $n - 2$ nd, which encodes the fact that p_{n-2} is one sector counterclockwise from p_{n-1} (and p_{n-1} and p_{n-2} are the endpoints of the edges e_1 and e_2 respectively). The polynomial \overline{B}_n has the same Hubbard tree as B_n but the invariant (counterclockwise) angle between e_2 and e_3 has measure $4\pi/3$. The complex kneading sequence for \overline{B}_n is $\overline{10 \cdots 01^*}$.

The families $K_{n,1}$ and $K_{n,2}$. The fourth and fifth families $K_{n,1}$ and $K_{n,2}$ have the same Hubbard tree and differ only by their invariant angle assignments. Unlike in the families A_n and B_n , this difference cannot be accounted for with complex conjugation. (As a consequence, we are in effect defining four families: $K_{n,1}$, $\overline{K}_{n,1}$, $K_{n,2}$, and $\overline{K}_{n,2}$.) The Hubbard tree for $K_{n,1}$ and $K_{n,2}$ is depicted in Figure 7c; we label e_1 as the edge between the p_0 and p_{n-1} . For $j \in \{1, 2\}$, the induced map on the edges of the Hubbard tree is given by:

$$(K_{n,j})_*(e_i) = \begin{cases} e_2 e_3 & i = 1 \\ e_{i+1} & 2 \leq i \leq n - 1 \\ e_1 e_2 & i = n \end{cases} .$$

The polynomial $K_{n,1}$ has cubic complex kneading sequence $\overline{1 \cdots 10^*}$. The (counterclockwise) angle between e_1 and e_2 has measure $2\pi/3$. This is indicated in the kneading sequence because the first digit is one more than the $(n - 1)$ st digit, which encodes the fact that p_1 is one sector counterclockwise from p_{n-1} (and p_{n-1} and p_1 are the endpoints of e_1 and e_2 , respectively).

The polynomial $K_{n,2}$ has cubic complex kneading sequence $\overline{1 \cdots 12^*}$. The (counterclockwise) angle between e_1 and e_2 has measure $4\pi/3$. This is indicated in the kneading sequence because the first digit is two more than the $(n - 1)$ st digit, which encodes the fact that p_1 is two sectors counterclockwise from p_{n-1} (and p_{n-1} and p_1 are the endpoints of e_1 and e_2 , respectively).

Both polynomials $K_{n,1}$ and $K_{n,2}$ map the post-critical set counterclockwise relative to the critical point.

While the polynomials $\overline{K}_{n,1}$ and $\overline{K}_{n,2}$ do not arise in the answer to the cubic twisted many-eared rabbit problem, we observe that both polynomials rotate the post-critical set clockwise with respect to the critical point. The kneading sequence for $\overline{K}_{n,1}$ is $\overline{1 \cdots 12^*}$ and the kneading sequence for $\overline{K}_{n,2}$ is $\overline{1 \cdots 10^*}$.

The family Y_n . Unlike the polynomials we have seen so far, the sixth and final family has a trivalent critical point. This is not possible for quadratic polynomials or polynomials with three post-critical points, so it does not have a direct analogue to any family of polynomials that appear in previously considered twisting problems. We call this family Y_n to reflect the trivalent critical point. The Hubbard tree for Y_6 is depicted in Figure 7d. The induced map on the edges of the Hubbard tree is given by:

$$(Y_n)_*(e_i) = \begin{cases} e_2 e_4 \cdots e_{2n-6} e_1 & i = 1 \\ e_3 e_4 & i = 2 \\ e_{i+2} & 3 \leq i \leq 2n - 7 \\ e_1 & i = 2n - 6 \\ e_1 & i = 2n - 5 \end{cases}.$$

The polynomial Y_n has cubic complex kneading sequence $\overline{120 \cdots 0}^*$. The critical point is valence 3 and the angle between each pair of edges that are adjacent in the cyclic order around the critical point is $2\pi/3$. The map Y_n permutes the vertices of Y_n counterclockwise with respect to the critical point. This is coarsely seen in the kneading sequence because the second digit is one more than the first and the $(n-1)$ st digit is one more than the $(n-2)$ nd, which encodes the fact that p_2 (and p_3, \dots, p_{n-2}) is one sector counterclockwise from p_1 and p_{n-1} is one sector counterclockwise from p_{n-2} .

On the other hand, the polynomial \bar{Y}_n has complex kneading sequence $\overline{10 \cdots 02}^*$. The map \bar{Y}_n permutes the vertices of \bar{Y}_n counterclockwise with respect to the critical point.

5.2. Reduction formulas. As in Section 3 (and Bartholdi–Nekrashevych [1]), the first step in solving the many-eared twisted cubic rabbit problem is to compute reduction formulas.

In what follows, we assume $n \geq 4$. The reduction formulas are as follows.

Let $m \in \mathbb{Z}$. Then

$$D_x^m R_n \simeq \begin{cases} D_x^k R_n & m = 9k \\ D_x R_n & m = 9k + 1 \\ D_x^2 R_n & m = 9k + 2 \\ D_y R_n & m = 9k + 3 \\ D_y D_x R_n & m = 9k + 4 \\ D_y^{-1} D_x^{-1} R_n & m = 9k + 5 \\ D_y^2 R_n & m = 9k + 6 \\ D_x^{-2} R_n & m = 9k + 7 \\ D_x^{-1} R_n & m = 9k + 8 \end{cases}.$$

The reduction formulas for the twisted many-eared cubic rabbit problem are similar to the reduction formulas for the twisted cubic rabbit problem from the previous section. Some of the calculations are in fact identical. The only cases that are different are when m is $9k+5$, $9k+6$, or $9k+8$. The difference in these cases is that when $n=3$, we have the lantern relation $D_z = D_y^{-1} D_x^{-1}$. The same relation does not hold when $n \geq 4$, which affects the calculation in two different ways. The first difference affects the base cases when $m = 9k+6$. If $n \geq 4$ and $m = 9k+6$, then $D_x^m R_n$ is equivalent to $D_y^{-1} D_x^{-1} R_n$. When $n=3$ and $m = 9k+6$, the same sequence of steps hold, but the lantern relation gives us that $D_y^{-1} D_x^{-1} R_n = D_z R_n$, which is equivalent to $D_x R_n$, hence yielding a different base case. The second difference arises when $m = 9k+5$ and $m = 9k+8$. The calculations for the reduction formulas when $m = 9k+5$

involve lifting the curve $D_y^{-1}D_x^{-1}(z)$ and the calculations for the reduction formulas when $m = 9k + 8$ involve lifting the curve $D_xD_y(z)$. When $n \geq 4$, the curves $D_y^{-1}D_x^{-1}(z)$ and $D_xD_y(z)$ both lift trivially, which allows these cases to reduce to a base case. On the other hand, when $n = 3$, the curves $D_y^{-1}D_x^{-1}(z)$ and $D_xD_y(z)$ are both equal to z (by the lantern relation), which results in the reduction formula D_x^k .

Before beginning our justifications of the reduction formulas, we observe several preliminary facts. For all $i \neq 1$ or 2 , we have $D_{c_i} \rightsquigarrow D_{c_{i-1}}$; in particular we have $D_{c_3} \rightsquigarrow D_{c_2} = D_x$. As in the case of R_3 , for all $n \geq 3$, the straight line arc b from the critical value p_1 to infinity is a special branch cut for R_n . We again have that $D_{D_y^k(z)} \rightsquigarrow \text{id}$ by Lemma 2.1. Unlike the case where $n = 3$, when $n \geq 4$ the curves x and z are disjoint and so the Dehn twists D_z and D_x commute; therefore $D_{D_x^k(z)} = D_z \rightsquigarrow D_{c_{n-1}}$. On the other hand, $D_{D_x^k(c_3)} \rightsquigarrow \text{id}$ when $k \not\equiv 0 \pmod{3}$ by Lemma 2.1.

Here are the calculations justifying the reduction formulas:

Case 1: $m = 9k$. We have $D_x^{9k} = (D_x^3)^{3k} \rightsquigarrow D_y^{3k} = (D_y^3)^k \rightsquigarrow D_z^k \rightsquigarrow \dots \rightsquigarrow D_x^k$.

Case 2: $m = 9k + 1$. As above, we use the fact that $D_{D_x^{-1}(y)}^3 \rightsquigarrow D_z$. We have:

$$D_x^{9k+1} \xrightarrow{D_x^2} D_y^{3k} D_x \xrightarrow{D_x^2} D_z^k D_x \xrightarrow{D_x^2} D_{c_{n-1}}^k D_x \xrightarrow{D_x^2} \dots \xrightarrow{D_x^2} D_{c_3}^k D_x \xrightarrow{D_x^2} D_x.$$

Case 3: $m = 9k + 2$. As above, we use the fact that the preimage of the curve $D_x^{-2}(y)$ has a single component, which is isotopic to z . We also use that D_x commutes with D_{c_i} for $i \neq 1$ or 3 . We have:

$$D_x^{9k+2} \xrightarrow{D_x^2} D_y^{3k} D_x^2 \xrightarrow{D_x^2} D_z^k D_x^2 \xrightarrow{D_x^2} \dots \xrightarrow{D_x^2} D_{c_3}^k D_x^2 \xrightarrow{D_x^2} D_x^2.$$

Case 4: $m = 9k + 3$. We have $D_x^{9k+3} \rightsquigarrow D_y^{3k+1} \xrightarrow{D_y} D_z^k D_y \xrightarrow{D_y} D_y$.

Case 5: $m = 9k + 4$. We have $D_x^{9k+4} \xrightarrow{D_x} D_y^{3k+1} D_x \xrightarrow{D_y D_x} D_z^k D_y D_x \xrightarrow{D_y D_x} D_y D_x$.

Case 6: $m = 9k + 5$. As above, we use two additional facts. First, the preimage of $D_x(y)$ is a single component that is homotopic to $D_y(z)$. Second, the curve $D_x D_y^2(z)$ has algebraic intersection 1 with b , therefore the preimage of $D_x D_y^2(z)$ is trivial by Lemma 2.1. We have

$$D_x^{9k+5} \xrightarrow{D_x^{-1}} D_y^{3k+2} D_x^{-1} \xrightarrow{D_y^{-1} D_x^{-1}} \psi(D_x D_y^{3k+3} D_x^{-1}) D_y^{-1} D_x^{-1} = (D_y D_z^{k+1} D_y^{-1}) D_y^{-1} D_x^{-1} \xrightarrow{D_y^{-1} D_x^{-1}}$$

$$\psi(D_x D_y^2 D_z^{k+1} D_y^{-2} D_x^{-1}) D_y^{-1} D_x^{-1} = D_y^{-1} D_x^{-1}.$$

Case 7: $m = 9k + 6$. We have $D_x^{9k+6} \rightsquigarrow D_y^{3k+2} \xrightarrow{D_y^2} D_z^k D_y^2 \xrightarrow{D_y^2} D_y^2$.

Case 8: $m = 9k + 7$. In this case we use the fact that the preimage of $D_x^2(y)$ consists of single connected component, which is homotopic to $D_x^{-1}(z)$:

$$D_x^{9k+7} \xrightarrow{D_x^{-2}} D_y^{3k+3} D_x^{-2} \xrightarrow{D_x^{-2}} D_y D_z^{k+1} D_y^{-1} D_x^{-2} \xrightarrow{D_x^{-2}} D_x^{-2}.$$

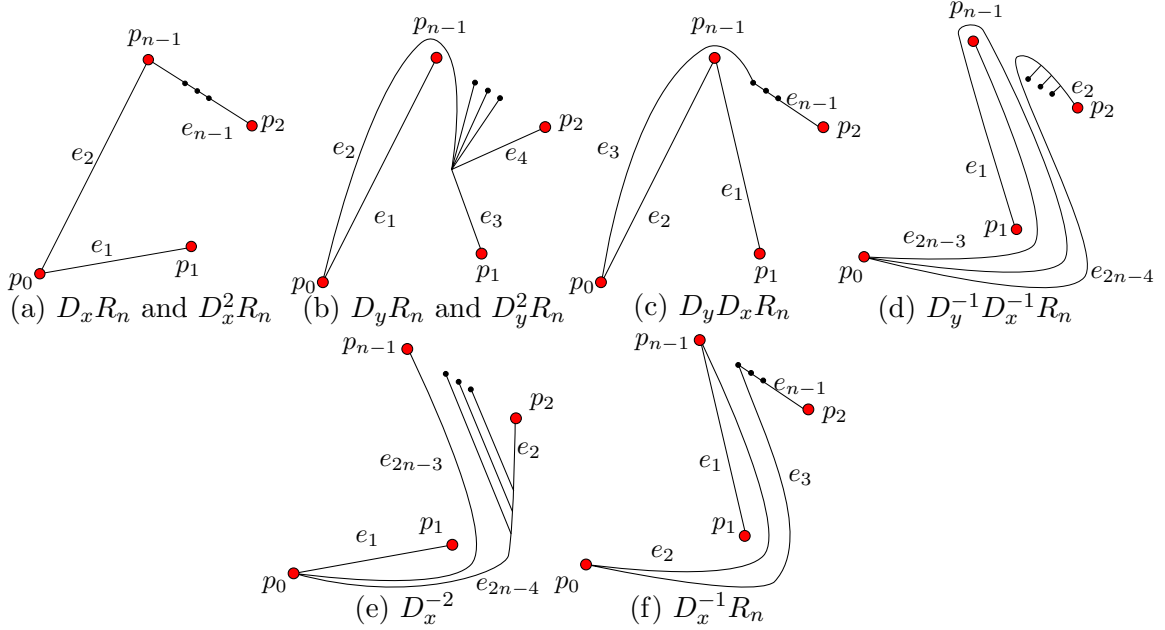


FIGURE 8. The topological Hubbard trees for the indicated maps.

Case 9: $m = 9k + 8$. In this case we use the fact that the preimage of the curve $D_x(y)$ consists of single connected component, which is homotopic to $D_y(z)$. We also use the fact that $D_y D_z D_y^{-1}$ lifts to the identity by Lemma 2.1. We have:

$$D_x^{9k+8} \underset{\sim}{\overset{D_x^{-1}}{\rightsquigarrow}} D_y^{3k+3} D_x^{-1} \underset{\sim}{\overset{D_x^{-1}}{\rightsquigarrow}} D_y D_z^{k+1} D_y^{-1} D_x^{-1} \underset{\sim}{\overset{D_x^{-1}}{\rightsquigarrow}} D_x^{-1}.$$

5.3. Base cases. To complete our solution to the twisted many-eared rabbit problem, it remains to determine the base cases.

Proof of Theorem 1.2. It follows from the reduction formulas that when $m \neq 0$ the map $D_x^m R_n$ is equivalent to one of the base cases, depending only on s , the first non-zero digit of the 9-adic expansion of m .

It remains to determine the polynomials to which the base cases are equivalent. We do this by applying the Alexander method [2, Proposition 3.1]. For each base case, let g be the twisted rabbit under consideration and let f be the polynomial to which we claim it is equivalent. We check that f and g are equivalent by checking that the preimage of the Hubbard tree for f is homeomorphic to the preimage of the topological Hubbard tree for g , that the invariant angle assignments of the trees are equal, and that the dynamical maps agree on the edges of the preimage trees. Topological Hubbard trees for each of the base cases are depicted in Figure 8. The maps $D_x R_n$ and $D_x^2 R_n$ have the same topological Hubbard tree, but the (counterclockwise) angle between e_1 and e_2 that is invariant under $D_x R_n$ is $2\pi/3$ and the angle that is invariant under $D_x^2 R_n$ is $4\pi/3$. Thus $D_x R_n$ is equivalent to A_n and $D_x^2 R_n$ is equivalent to \bar{A}_n . The maps $D_y R_n$ and $D_y^2 R_n$ have the same topological Hubbard tree, but the (counterclockwise) angle between e_1 and e_2 that is invariant under $D_y R_n$ is $\frac{2\pi}{3}$ and the invariant angle under $D_y^2 R_n$ is $\frac{4\pi}{3}$. Indeed, the bottom row of Figure 9 demonstrates the process of lifting the topological Hubbard for $D_y R_n$ through the map $D_y R_n$. Moreover, it also shows that the edges of the lift of the topological Hubbard tree that are homotopic (relative to endpoints) to e_1 and e_2 have angle measure $\frac{2\pi}{3}$. Thus $D_y R_n$ is equivalent to $K_{n,1}$

and a similar calculation shows that $D_y^2 R_n$ is equivalent to $K_{n,2}$. The topological Hubbard tree for $D_y D_x R_n$ is a path of length $n - 1$ with the same edge map as B_n , and indeed the angle between e_2 and e_3 (measured counterclockwise) is $\frac{2\pi}{3}$. Therefore $D_y D_x R_n$ is equivalent to B_n . On the other hand, the topological Hubbard tree for $D_x^{-1} R_n$ has the same edge map as B_n , but the (counterclockwise) angle between e_2 and e_3 is $\frac{4\pi}{3}$. Therefore $D_x^{-1} R_n$ is equivalent to \overline{B}_n . The topological Hubbard tree for $D_y^{-1} D_x^{-1} R_n$ is trivalent at the critical point and the edges $\{e_1, e_{2n-3}, e_{2n-4}\}$ are cyclically permuted counterclockwise, which agrees with the edge map for \overline{Y}_n . Similarly, the topological Hubbard tree for $D_x^{-2} R_n$ is also trivalent at the critical point. However, $D_x^{-2} R_n$ permutes the edges $\{e_1, e_{2n-3}, e_{2n-4}\}$ cyclically permutes the edges clockwise, which agrees with the edge map for Y_n . \square

As mentioned in Section 5 of [2], the tree lifting algorithm is used to find the topological Hubbard tree for each base case. Once found, however, the earlier steps of the algorithm are not needed in order to verify that the output tree is invariant under lifting. We illustrate both the algorithm and the invariance check for the map $D_y R_n$ from case $9k + 3$ in Figure 9. Using the Hubbard tree for R_n as the input tree, the tree lifting algorithm requires only a single step in order to find the topological Hubbard tree for $D_y R_n$.

More generalizations. Notice that because each of c_3, c_4, \dots, c_{n-1} and $c_0 = z$ lifts to x under iteration of the lifting map for R_n , we have that $D_{c_i}^m \simeq D_x^m$ for all $i \neq 1$ and for all $m \in \mathbb{Z}$. Thus our solution to the twisted rabbit problems of the form $D_x^m R_n$ also immediately give solutions to all twisted rabbit problems of the form $D_{c_i}^m R_n$ with $i \neq 1$.

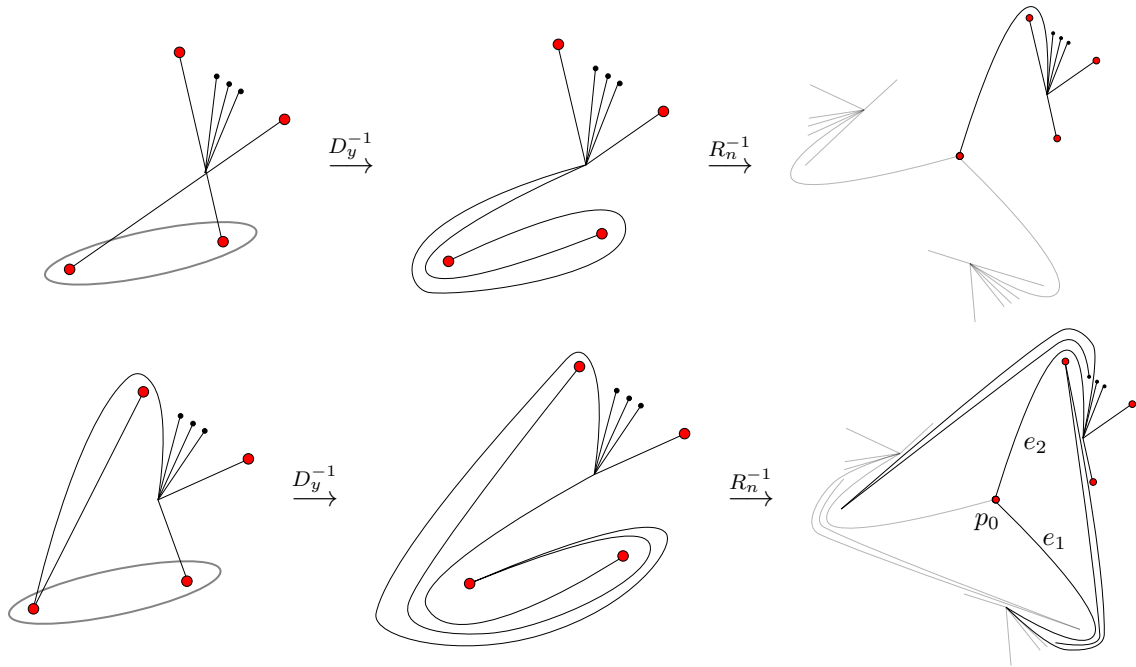


FIGURE 9. The top row shows the lift of the Hubbard tree for R_n under $D_y R_n$. The second row shows that the resulting tree is invariant under $D_y R_n$. In the figures on the right, the dark edges are those that are in the hull of the post-critical set.

REFERENCES

- [1] Laurent Bartholdi and Volodymyr Nekrashevych. Thurston equivalence of topological polynomials. *Acta Math.*, 197(1):1–51, 2006.
- [2] James Belk, Justin Lanier, Dan Margalit, and Rebecca R. Winarski. Recognizing topological polynomials by lifting trees. To appear in *Duke Math. J.*, 2022.
- [3] A. Douady and J. H. Hubbard. *Étude dynamique des polynômes complexes. Partie I*, volume 84 of *Publications Mathématiques d’Orsay [Mathematical Publications of Orsay]*. Université de Paris-Sud, Département de Mathématiques, Orsay, 1984.
- [4] A. Douady and J. H. Hubbard. *Étude dynamique des polynômes complexes. Partie II*, volume 85 of *Publications Mathématiques d’Orsay [Mathematical Publications of Orsay]*. Université de Paris-Sud, Département de Mathématiques, Orsay, 1985. With the collaboration of P. Lavaurs, Tan Lei and P. Sentenac.
- [5] Benson Farb and Dan Margalit. *A primer on mapping class groups*. Princeton University Press, 2011.
- [6] John H. Hubbard and Dierk Schleicher. The spider algorithm. In *Complex dynamical systems (Cincinnati, OH, 1994)*, volume 49 of *Proc. Sympos. Appl. Math.*, pages 155–180. Amer. Math. Soc., Providence, RI, 1994.
- [7] Virpi Kauko. Shadow trees of Mandelbrot sets. *Fund. Math.*, 180(1):35–87, 2003.
- [8] Silvio Vieira Ferreira Levy. *Critically finite rational maps (Thurston)*. ProQuest LLC, Ann Arbor, MI, 1985. Thesis (Ph.D.)—Princeton University.
- [9] Y. Muntyan and D. Savchuk. AutomGrp, automata groups, Version 1.3.2. <https://gap-packages.github.io/automgrp>, Sep 2019. Refereed GAP package.
- [10] Volodymyr Nekrashevych. *Self-similar groups*, volume 117 of *Mathematical Surveys and Monographs*. American Mathematical Society, Providence, RI, 2005.
- [11] Alfredo Poirier. Hubbard trees. *Fund. Math.*, 208(3):193–248, 2010.

JUSTIN LANIER, DEPARTMENT OF MATHEMATICS, UNIVERSITY OF CHICAGO, 5734 S. UNIVERSITY AVENUE, CHICAGO, IL 60637

Email address: `jlanier8@uchicago.edu`

REBECCA R. WINARSKI, DEPARTMENT OF MATHEMATICS AND COMPUTER SCIENCE, COLLEGE OF THE HOLY CROSS, 1 COLLEGE STREET, WORCESTER, MA 01610

Email address: `rebecca.winarski@gmail.com`